Science Advances
AAAS

advances.sciencemag.org/cgi/content/full/6/47/eabc3207/DC1

Supplementary Materials for

A 3D culture platform enables development of zinc-binding prodrugs for targeted proliferation of β cells

Kisuk Yang, Miseon Lee, Peter Anthony Jones, Sophie S. Liu, Angela Zhou, Jun Xu, Vedagopuram Sreekanth, Jamie L. Y. Wu, Lillian Vo, Eunjee A. Lee, Ramona Pop, Yuhan Lee, Bridget K. Wagner, Douglas A. Melton, Amit Choudhary*, Jeffrey M. Karp*

*Corresponding author. Email: jeffkarp@mit.edu (J.M.K.); achoudhary@bwh.harvard.edu (A.C.)

Published 18 November 2020, *Sci. Adv.* **6**, eabc3207 (2020)
DOI: 10.1126/sciadv.abc3207

This PDF file includes:

Supplementary Texts S1 and S2
Supplementary Materials and Methods
Figs. S1 to S9
Table S1
References

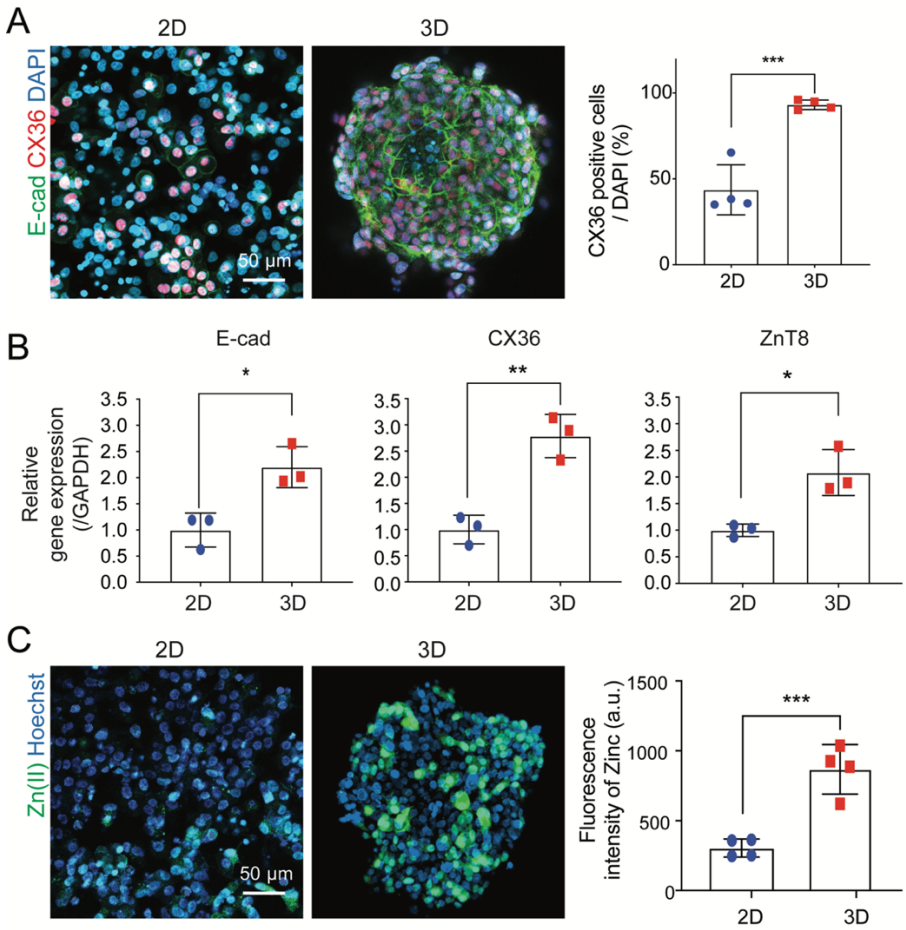

Fig. S1. A discrepancy exists between key cell junction markers and zinc levels of stem cell derived β cells (SC β cells) in 2D and 3D culture systems.

(A) Representative images and quantification of connexin 36 (CX36) positive SC β cells. 3D culture system [e.g., spinner flask (SF)] shows increased β-cell expression of junction markers, E-cadherin (E-cad) and CX36 compared with monolayered 2D culture condition. Nuclear back stained with DAPI ($n = 4$, ***$p < 0.001$ versus 2D).

(B) Quantitative real-time polymerase chain reaction (qRT-PCR) analyses examine the expression of E-cad, CX36, and zinc transporter 8 (ZnT8) in SC β cells were cultured for 2 days before analysis. SC β cells in 3D (SF) show a significantly higher gene expression profile of E-cad, CX36, and ZnT8 versus 2D systems. ($n = 3$, *$p < 0.05$, **$p < 0.01$ versus 2D).

(C) 3D system (SF) for SC β cell culture contains higher Zn(II) levels than 2D group as seen by representative images and fluorescence intensity measured by FluoZin™-3 indicator dye ($n = 4$, ***$p <$ 0.001 versus 2D).

Supplementary Text 1

Motivation for developing a new 3D screening system

Within the pancreas, β cells are dispersed in islets of Langerhans that consist of endocrine cells, vascularisations, neuronal cells and extensive cell-cell interactions generating a highly distinct pancreatic

niche to support β cell function and viability (*19*). Specifically, adherent junctions (e.g., E-cad) initiate cell-cell contacts and maintain cell structure cohesiveness, while gap junctions (e.g., CX36) regulate cell-cell signaling pathways that are important for insulin synthesis and release through the exchange of current-carrying ions between cells (*46-48*). However, currently existing 2D screening systems often insufficiently recapitulate the cell-cell interactions, junction protein, and zinc levels essential for the proper functioning and insulin secretion of β-cell islets (*11*), therefore making them inaccurate for screening and differentiating hits within a small molecule library (*49-51*).

Due to the nature of our proposed zinc chelators, testing in β cells required physiological zinc levels for understanding and differentiating the effects of a zinc-binding prodrugs (ZnPD). Therefore, prior to synthesizing and screening ZnPDs, we hypothesized that single cells in 2D would have disrupted cell-cell interactions leading to decreased cell function and zinc levels, making them an inappropriate screening platform for developing our technology. We initially investigated whether 2D conventional culture systems could support the cellular and biophysical environment for accurate screening by comparing levels of key systems between 2D and the benchmark 3D culture system. As the 3D system, we chose the most widely used for maintaining and differentiating large batches of SC β cells, the SF, which can provide a tunable, continuous fluid shear stress to support cell aggregates at similar sizes as SC β clusters. Comparing monolayered 2D and 3D (SF) systems, immunofluorescent staining and qRT-PCR analyses revealed significantly decreased gene expression of junction protein markers (E-Cad and CX36) in SC β cells in the 2D group compared to the 3D group (fig. S1A, B). By establishing that cell-cell contacts were increased in 3D culture systems, we then investigated whether Zn(II) and zinc transporters, which are vital for cell-cell signaling and zinc-insulin crystallization within secretory vesicles, were also increased in 3D systems (*11*). Correspondingly, the gene expression of ZnT8, which transports Zn(II) for crystallization and storage of insulin (*52*), was also significantly increased in islets cultured in 3D (fig. S1B). Intracellular zinc fluorescent intensity from cells in both 2D and 3D group were measured, and the conventional 2D culture system showed significantly lower the Zn(II) than the 3D system (2D: 304.8 ± 64.5 and 3D: 867.3 ± 176.5, 0.35 fold versus 3D) (fig. S1C). These data suggest that 3D culture environments would provide a more accurate β-cell phenotype to more reliably screen ZnPDs.

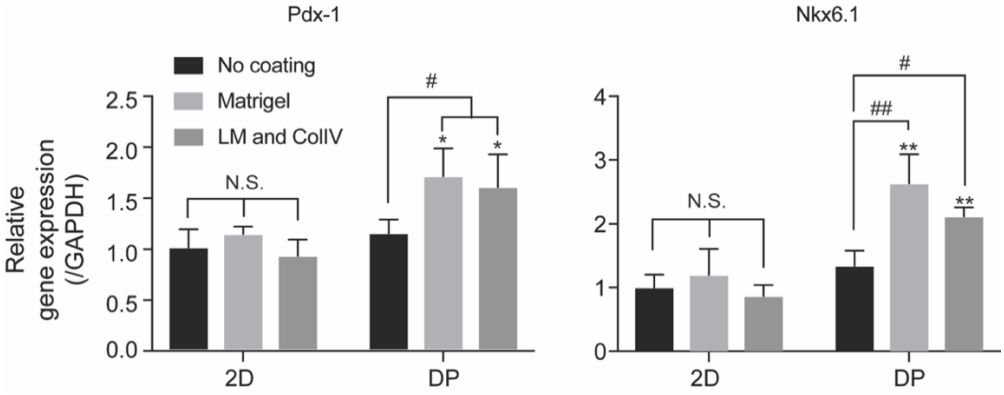

Fig. S2. Cell discs in Disque platform (DP) re-establish cell-extracellular matrix (ECM) interactions which are critical for pancreatic differentiation. Gene expression of pancreatic and duodenal homeobox 1 (Pdx-1) and NK6 homeobox 1 (Nkx6.1) from pancreatic progenitor (PP) cells cultured on DP pre-coated with Matrigel or Laminin (LM) / Collagen IV (ColIV) for 4 days (n=3, *p<0.05, **p<0.01 versus 2D No coating, #p<0.05, ##p<0.01 versus DP No coating).

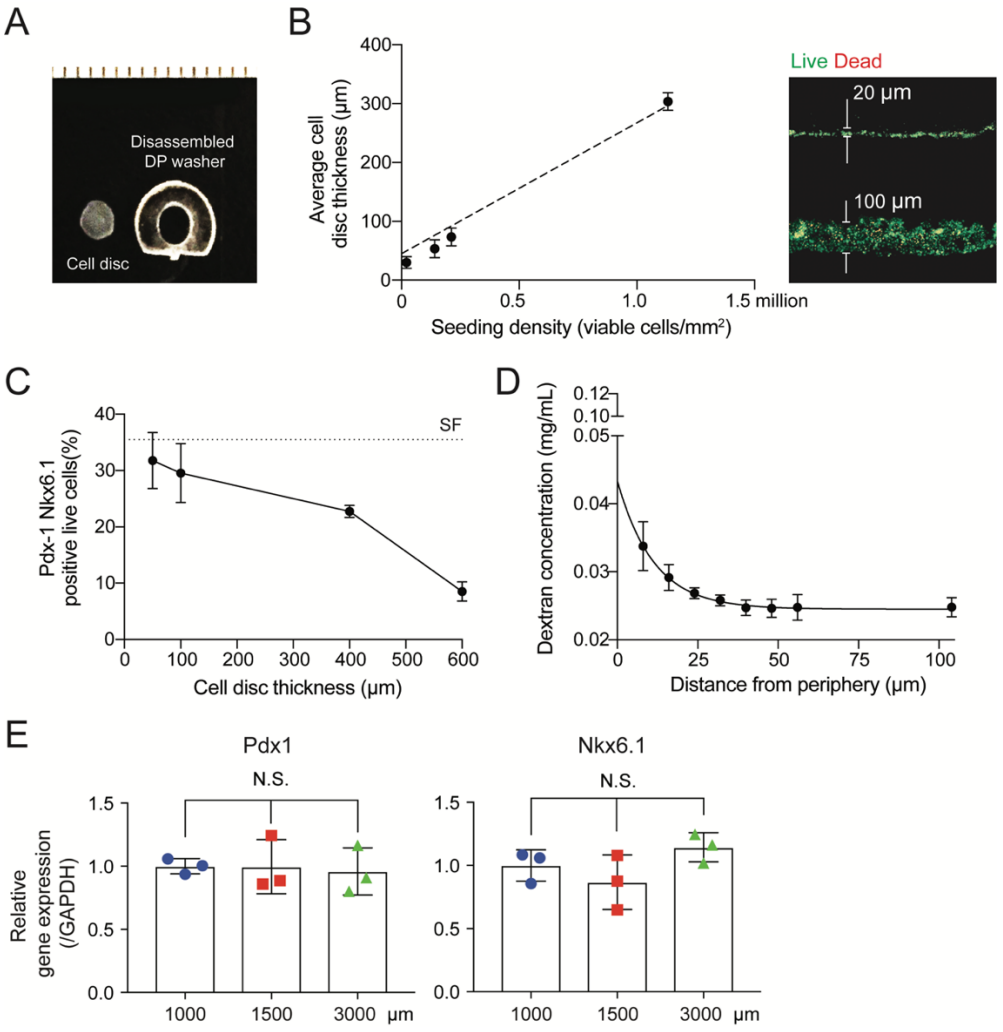

Fig. S3. Optimization of thickness and diameter of the cell discs in DP for nutrient diffusion and differentiation of the cells.

(A) Representative image showing a cell disc disassembled from a DP washer.
(B) Correlation between the seeding density and the estimated disc thickness (n=3), with representative immunofluorescent images showing the side views of cell discs stained with Live/Dead assay.
(C) Correlation between the thickness in cell disc and the percentage of cells with co-expression of Pdx-1 and Nkx6.1 after 4 day differentiation [stage 4 day 1 (S4d1) to S4d5)] (n=3).
(D) Dextran diffusion within SC β clusters taken from SF suspension culture, after a 4 hour incubation in 0.125 mg/ml 10-kDa Texas Red™-dextran (n=3).
(E) Gene expression of PP cells for Pdx-1 and Nkx6.1 after 4 days (S4d1 to S4d5) grown in 1000, 1500, and 3000 μm diameter DPs (n=3).

Supplementary Text 2

Optimization of thickness and diameter of the cell discs in DP

While size-controlled pseudo islets have been developed using various islet sources, e.g. Aggrewell™, these pseudo islets are still susceptible to necrotic core development (*53*). This has ultimately limited the diameters of these islets (less than 100 μm) in order to maintain homogenous viability. Thus, in this study we focused on developing disc-like cell aggregates to maximize surface area for oxygen and nutrient diffusion with regulated cell thicknesses and homogenously maintain cell viability. To determine optimal dimensions and seeding density of cell discs in the DP, we linearly controlled the thickness of the cell discs to observe homogenous distribution of cells within the Disques (fig. S3A, B). Although the cells were centrifuged to achieve a rapid spatial re-arrangement in the Disques, we found that their viability profile was not extensively compromised at low disc thicknesses. After PP cells were differentiated to the end of stage 4, the co-expression of Pdx-1 and Nkx6.1 (*54*) was comparable between 50-μm cell discs and 3D islets from the current gold-standard suspension flask culture system (SF) (fig. S3C). As the thickness increased (50 ~ 600 μm), both the viability and differentiation potentials of the SC β cells reduced (fig. S3B, C). As a known challenge to cultured embryoids and cell spheroids (*55-57*), we hypothesized this might be due to the diffusion gradient from the periphery to the center of cell discs, especially for the high-molecular-weight growth factors that were supplemented during β-cell differentiation, such as activin A (26.2 kDa), KGF (18.9 kDa), and β-cellulin (10 ~ 15 kDa). We tested this using a 10-kDa Texas Red™-dextran probe and imaged by confocal microscopy. For imaging, the clusters were fixed and cryosectioned. Fluorescence intensity was measured, which showed a diffusive gradient through the outermost 50 μm of SC β clusters, which was consistent with the diffusion limit observed in literature (fig S3D) (*58*). Here, the 50 μm-thick discs may

show better diffusion than islets cultured in SF (i.e., 25 µm from each exposed side). However, cell behavior does not only depend on 10-kDa sized nutrient diffusion. Other growth factors, biomolecules, and proteins of different sizes may be expected to influence β cell behavior such as viability, differentiation, and function.

On the other hand, the diameter of cell discs (1,000 ~ 3,000 µm) had minimal influence on the expression of key β-cell markers (Nkx6.1 and Pdx-1) (fig S3E). Ultimately, we decided to seed at a density of 0.8 x 10^6 cells/Disque (50 µm thickness). If the cells were to be seeded directly in the wells of 96-plate, each well would require ~3.6 million cells *(44)*. However, the use of the Disque apparatus has restricted the diameter of each cell disc to 3.0 mm and overall reduced the number of cells by ~4.5-fold. To support the diffusion of nutrient to this densely packed cell disc, the pedestal design in the Disque apparatus enables dual-direction media diffusion to maintain cell viability.

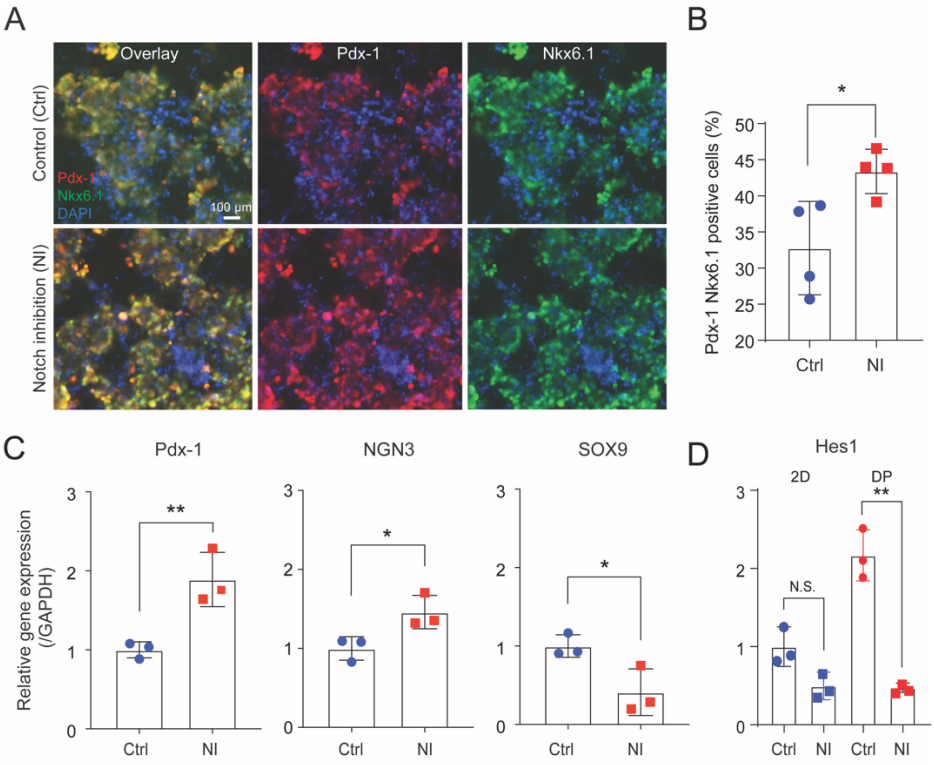

Fig. S4. Assessing the behavior of PP cell differentiation in response to notch signaling inhibition in DP. PP cells in DP were treated with notch inhibitor (NI, ɣ-secretase inhibitor, N-[N-(3,5-Difluorophenacetyl)-L-alanyl]-S-phenylglycine t-butyl ester (DAPT), 10 µM) for 4 days in culture.
(A) Immunofluorescent staining for Pdx-1 and Nkx6.1 markers.
(B) The relative proportion of Pdx-1 and Nkx6.1 co-positive cells in the DPs (n=4, *p<0.05 versus control).
(C) qRT-PCR analyses to determine the gene expression of Pdx-1, Neruogenin3 (NGN3) and SOX9 markers in PP cells cultured in DP (n = 3, *p<0.05, **p<0.01 versus control).

(D) Gene expression profiles for hairy and enhancer of split-1 (Hes1) in the cells in both 2D and DP (n=3, **p<0.01 versus DP control).

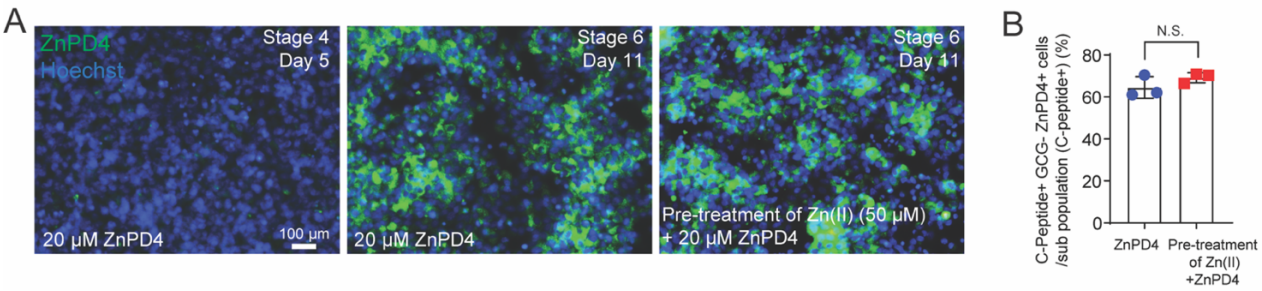

Fig. S5. Selective unmasking of ZnPD4 in SC β cells.
(A) Representative images showing the selective unmasking of ZnPD4 (20 μM) in PP cells (S4d5) and SC β cells (S6d11). The SC β cells in the right most panel was pre-treated with Zn(II) (50 μM) 1 day before in culture media. Hoechst nuclear back stain.
(B) Propensity of SC β cells (C-peptide+, GCG-, and ZnPD4+) treated with ZnPD4 with or without pre-treatment of Zn(II) (50 μM) 1 day before in culture media, quantified by flow cytometry (n=3).

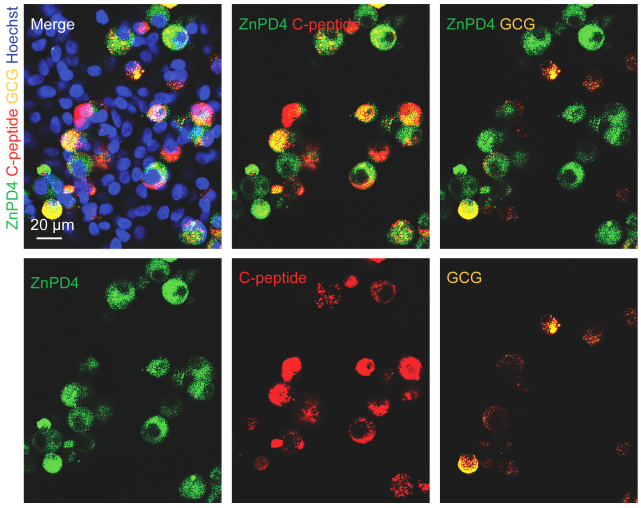

Fig. S6. Representative images showing the selective unmasking of ZnPD4 (20 μM) in SC β cells stained with C-peptide and glucagon (GCG). Hoechst used as nuclear back stain.

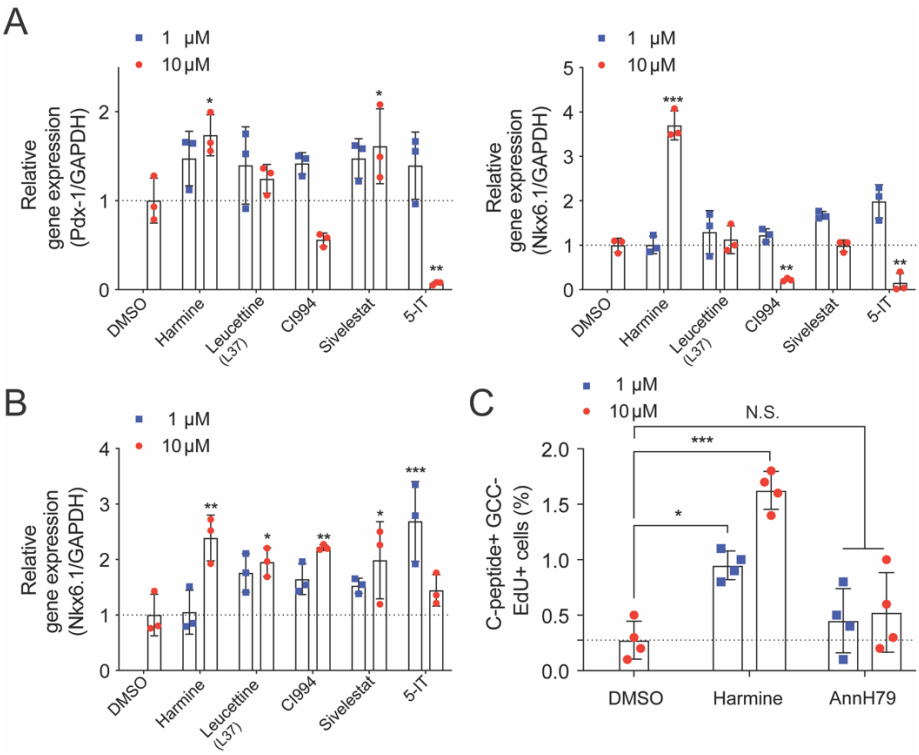

Fig. S7. Harmine and other β cell proliferation inducing parent small molecules are screened in both (A) PP and (B) SC β cells; (C) harmine emerged as the most efficacious for driving PP cell differentiation into mono hormonal SC β cells.

(A) Gene expression of Pdx-1 and Nkx6.1 in PP cells treated in the DP identified harmine as a viable candidate. The β cell proliferation agents were treated at 1 and 10 μM (n = 3, *p < 0.05, **p < 0.01, ***p<0.001 versus DMSO).

(B) Gene expression of Nkx6.1 in SC β cells treated in the DP consistently identified harmine as a viable candidate for inducing β-cell differentiation and function. β cell proliferation agents were treated at 1 and 10 μM (n = 3, *p < 0.05, **p < 0.01, ***p<0.001 versus DMSO).

(C) Flow cytometry data quantified proliferation (EdU+) of SC β cells (C-peptide+ GCG-) after treatment of the harmine in the DP. AnnH79 is a harmine analog used as a negative control (n = 4, *p<0.05, ***p<0.001 versus DMSO).

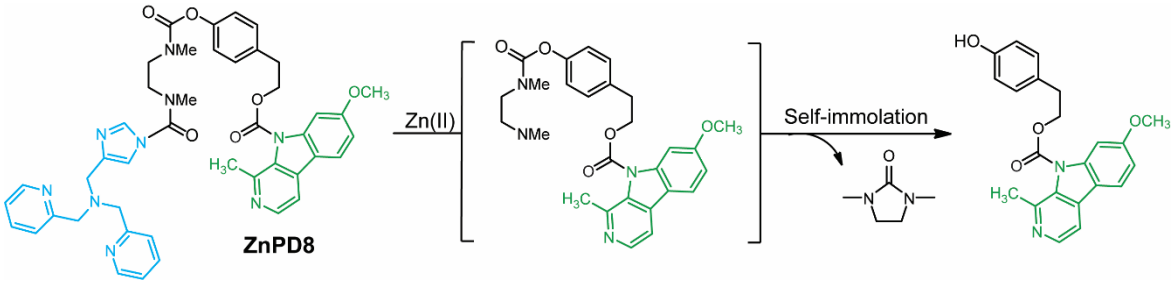

Fig. S8. Proposed mechanism of ZnPD8. Proposed mechanism of Zn(II)-mediated hydrolysis of ZnPD8 which serves as a negative control because it does not release the active cargo.

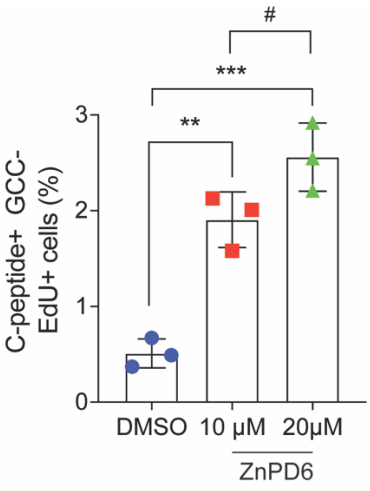

Fig. S9. Comparison of ZnPD6 dosage between 10 and 20 μM in the population of proliferating SC β cells (C-peptide+ GCG- EdU+) (n=3, *p < 0.05, **p < 0.01, ***p < 0.001 versus DMSO, #p < 0.05 versus 10 μM ZnPD6).

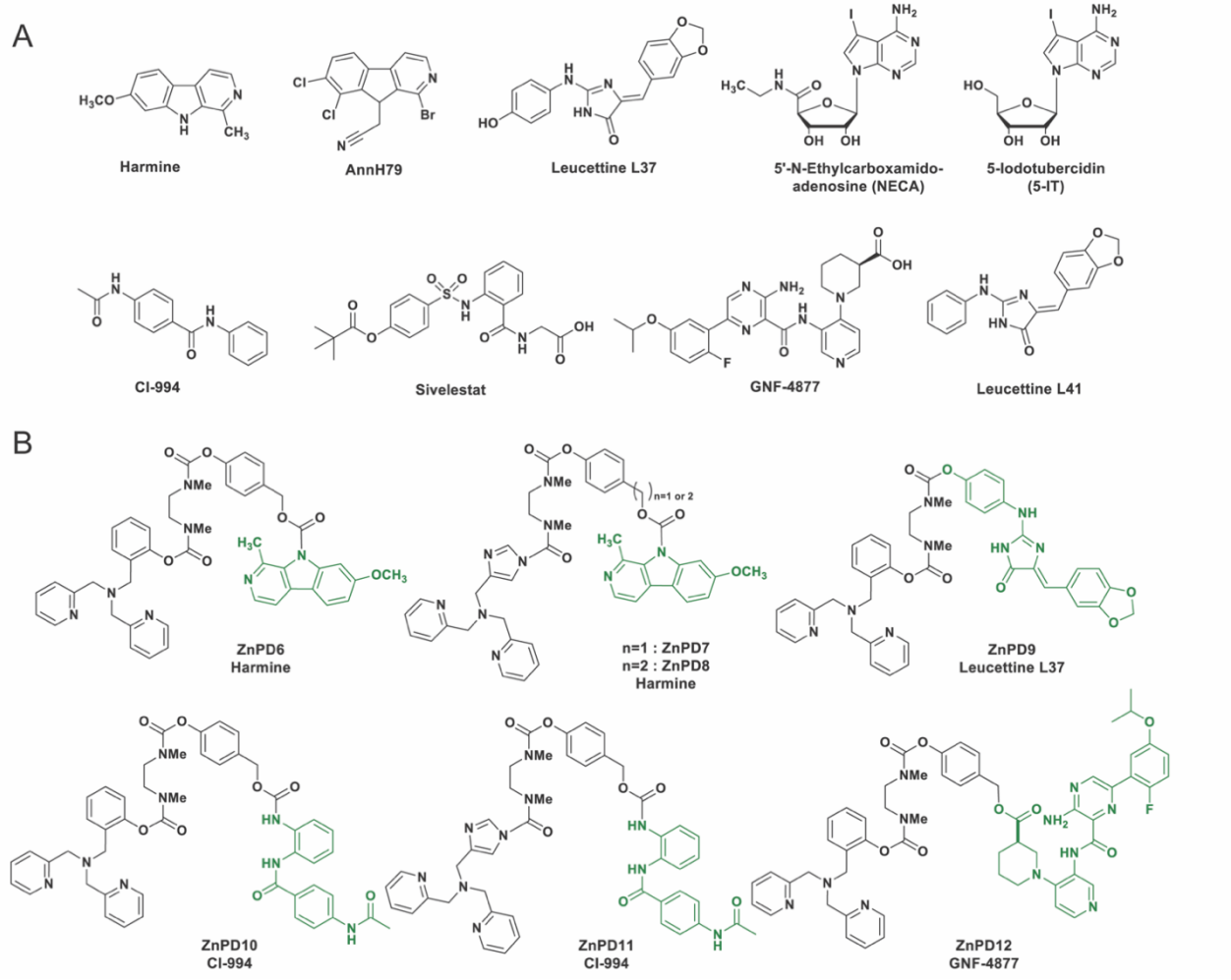

Table S1. Chemical structure of small molecules and ZnPDs.

(A) List of known β cell proliferating small molecules.

(B) List of ZnPDs: known β cell proliferating small molecules appended to zinc chelating system.

Supplementary Materials and Methods

All reagents were purchased and used as received from commercial sources without further purification. Reactions were performed in round-bottom flasks stirred with Teflon®-coated magnetic stir bars. Moisture and air-sensitive reactions were performed under a dry nitrogen/argon atmosphere. Moisture and air-sensitive liquids or solutions were transferred *via* nitrogen-flushed syringes. As necessary, organic solvents were degassed by bubbling nitrogen/argon through the liquid. The reaction progress was monitored by thin-layer chromatography (TLC) and ultra-performance liquid chromatography mass spectrometry (UPLC-MS). Flash column chromatography was performed using silica gel (60 Å mesh, 20–40 μm) on a Teledyne Isco CombiFlash Rf system. Analytical TLC was performed using Merck Silica gel 60 F254 pre-coated plates (0.25 mm); illumination at 254 nm allowed the visualization of UV-active material, and a phosphomolybdic acid (PMA) stain was used to visualize UV-inactive material. UPLC-MS was performed on a Waters ACQUITY UPLC I-Class PLUS System with an ACQUITY SQ Detector 2. Nuclear magnetic resonance (NMR) spectra were recorded on a Bruker 400 Spectrometer (^{1}H NMR, 400 MHz; ^{13}C, 100 MHz) at the Broad Institute of MIT and Harvard. ^{1}H and ^{13}C chemical shifts are indicated in parts per million (ppm) relative to SiMe4 (δ = 0.00 ppm) and internally referenced to residual solvent signals. NMR solvents were purchased from Cambridge Isotope Laboratories, Inc., and NMR data were obtained in $CDCl_3$. Data for ^{1}H NMR are reported as follows: chemical shift value in ppm, multiplicity (s = singlet, d = doublet, t = triplet, dd = doublet of doublets, and m = multiplet), integration value, and coupling constant value in Hz.

Synthesis of linkers and Zinc-chelating ligand

The linker was prepared as described by Gillies et al., and the spectroscopy data was matched as reported

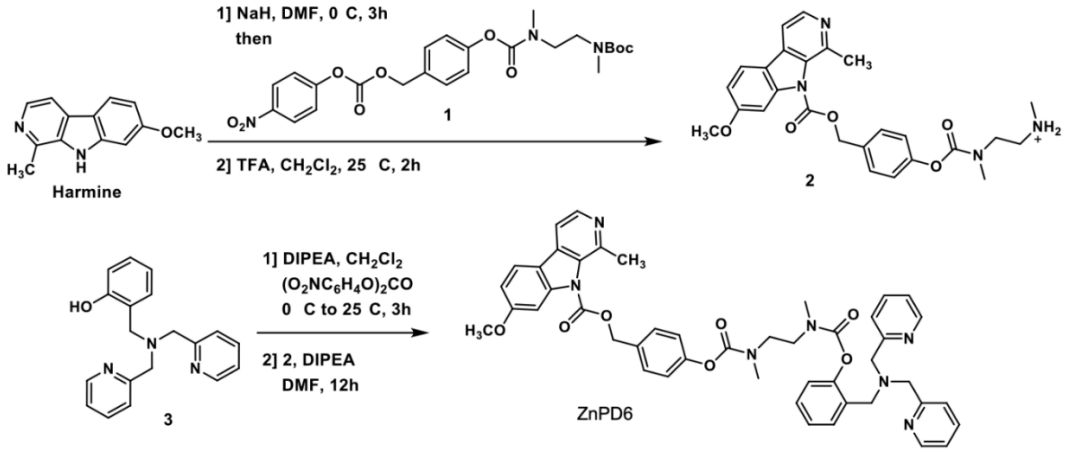

(*59*). The zinc-chelating ligand (compounds 3 and 6) were prepared as described by Nam et al., and Karlin et al. The spectroscopy data were matched with a report (*60,61*).

Synthetic route for ZnPD6

The NaH (52.8 mg, 1.32 mmol) was added to the solution of Harmine (140mg, 0.66mmol) in anhydrous dimethylformamide (4.12 mL, 0.1M) at 0 °C and the reaction was stirred at the same temperature for 2 hours. The linker (431.8 mg, 0.86 mmol) was dissolved in anhydrous dimethylformamide (3.0 mL) and added to the reaction mixture. The reaction was slowly warmed to room temperature and stirred for 12 hours. The reaction was quenched with an aqueous solution of saturated $NaHCO_3$ and extracted with dichloromethane. The organic layers were combined, washed with brine, dried over anhydrous Na_2SO_4, filtered, and concentrated in vacuo to give a crude residue, which was purified by flash column chromatography on silica gel, eluting with methanol in dichloromethane. The pale yellow foam product (compound 2) was obtained (248.5 mg, 64%) and carried forward to the next step. The carbamate (248.5 mg, 0.43 mmol) was dissolved in anhydrous dichloromethane (4.34 mL, 0.1 M) then trifluoroacetic acid (370 mg, 3.25 mmol) was added to the reaction mixture. The solution was stirred for 2 hours. The solvent was removed in vacuo, and dichloromethane was successively added and evaporated to remove residual trifluoroacetic acid and to provide the deprotected product. This product was carried over to the next step without further purification, wherein 4-nitrophenyl carbonate (157.4 mg, 0.52 mmol) and N,N-diisopropylethylamine (83.6 mg, 0.65

mmol) were added to the solution of zinc chelating ligand 3 (131.6 mg, 0.43 mmol) in dichloromethane (4.31 ml, 0.1M) at 0 °C. The reaction mixture was slowly warmed up to room temperature over 3 hours. N,N-diisopropylethylamine (334.2 mg, 2.59 mmol) and trifluoroacetic acid salt of compound 2 (0.43 mmol) in dimethylformamide (3 ml) were added to the reaction mixture and stirred for 12 hours at room temperature . The solvent was removed in vacuo, and the residue was purified by flash column chromatography eluting with 0 to 10% methanol in dichloromethane (1% NH_4OH) to give the pure fraction of ZnPD6 as a yellow foam (91.3mg, 26% yield). ^{1}H NMR (400 MHz, $CDCl_3$) δ 8.52 – 8.48 (m, 2H), 8.46 (d, *J* = 5.1 Hz, 1H), 7.84 (d, *J* = 8.6 Hz, 1H), 7.71 – 7.57 (m, 5H), 7.57 – 7.43 (m, 4H), 7.24 – 7.09 (m, 6H), 6.99 (ddd, *J* = 19.6, 8.0, 2.2 Hz, 2H), 5.48 (S, 2H), 3.85 – 3.73 (m, 7H), 3.73 – 3.53 (m, 6H), 3.17 -3.02 (m, 6H), 2.72 (S, 3H). ^{13}C NMR (100 MHz, $CDCl_3$) δ 161.7, 159.8 (2C), 151.8, 149.9, 149.1 (2C), 146.7, 143.5, 141.9, 136.6, 134.4, 134.1, 131.6, 131.4, 130.5, 130.4(2C), 130.3, 130.2, 128.1, 125.9, 122.9(2C), 122.6(2C), 122.4, 122.1(2C), 121.9, 117.8, 112.8, 111.2, 100.3, 69.0, 60.5, 60.4, 55.8(2C), 52.5, 47.8, 47.0, 35.6, 35.4, 35.3, 25.3.

Synthesis of ZnPD7-8

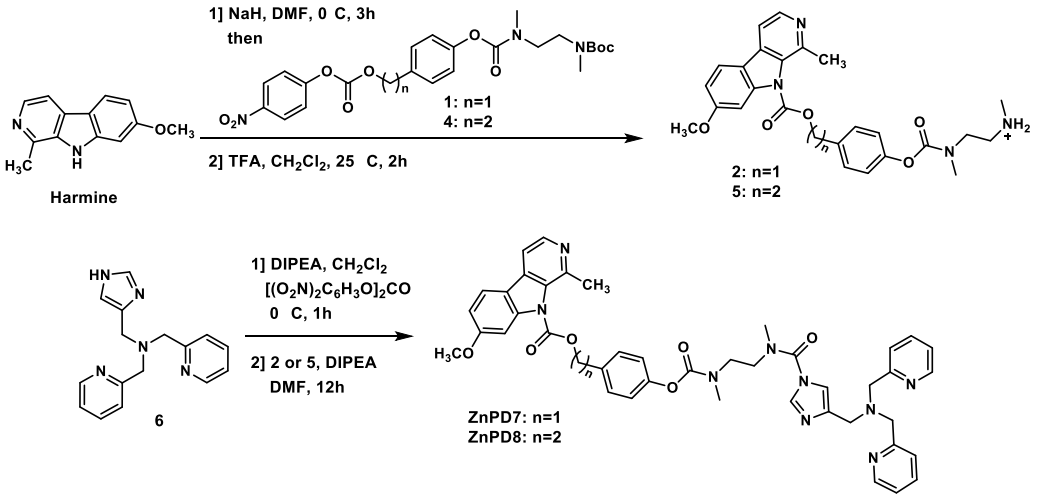

Synthetic route for ZnPD7-8

ZnPD7: The compound 2 was carried over to the next step without further purification, wherein 4-nitrophenyl carbonate (157.4 mg, 0.52 mmol) and N,N-diisopropylethylamine (83.6 mg, 0.65 mmol) were added to the solution of zinc chelating ligand 3 (131.6 mg, 0.43 mmol) in dichloromethane (4.31 ml) at 0 °C. The reaction mixture was slowly warmed up to room temperature over 3 hours. N,N-diisopropylethylamine (334.2 mg, 2.59 mmol) and trifluoroacetic acid salt of compound 2 (0.43 mmol) in dimethylformamide were added to the reaction mixture and stirred for 12 hours at room temperature . The solvent was removed in vacuo, and the residue was purified by flash column chromatography eluting with 0 to 10% methanol in dichloromethane (1% NH_4OH) to give the pure fraction of ZnPD7 as a pale yellow foam (91.1mg, 27.1% yield). ^{1}H NMR (400 MHz, $CDCl_3$) δ 8.50 (t, *J* = 5.1 Hz, 2H), 8.45 (d, *J* = 5.1 Hz, 1H), 7.87 – 7.80 (m, 2H), 7.66 – 7.54 (m, 6H), 7.46 (t, *J* = 9.0 Hz, 2H), 7.25 – 7.23 (m, 1H), 7.16 – 7.03 (m, 4H), 6.96 (dd, *J* = 8.6, 2.3 Hz, 1H), 5.46 (d, *J* = 5.0 Hz, 2H), 3.85 (s, 4H), 3.79 (d, *J* = 5.9 Hz, 3H), 3.75 – 3.61 (m, 6H), 3.16 (m, 3H), 3.04 (m, 3H), 2.71 (s, 3H). ^{13}C NMR (100 MHz, $CDCl_3$) δ 161.7, 159.8, 155.3, 154.1, 152.1, 151.9, 151.8, 149.2(2C), 146.7, 143.5, 141.9, 140.2, 139.9, 137.0, 136.9, 136.6, 134.3, 134.1, 131.9, 130.5, 130.4(2C), 123.1, 122.3, 122.0, 121.9, 117.8, 116.7, 112.8, 111.2, 100.3, 69.0, 59.9(2C), 55.8, 51.4, 47.7, 46.5, 37.6, 35.5, 35.1, 25.3.

ZnPD8: The compound 5 was synthesized in the same way as described in ZnPD5 synthesis. The synthesis of ZnPD8 was carried the same as ZnPD7 synthesis. ZnPD7 as a pale yellow foam (118 mg, 29.2 % yield). ^{1}H NMR (400 MHz, $CDCl_3$) δ 8.46 (d, *J* = 4.8 Hz, 2H), 8.42 (d, *J* = 5.1 Hz, 1H), 7.83 – 7.77 (m, 2H), 7.62 – 7.52 (m, 6H), 7.25 – 7.13 (m, 3H), 7.10 – 7.02 (m, 2H), 7.01 – 6.87 (m, 3H), 4.62 (t, *J* = 7.3 Hz, 2H), 3.82 (d, *J* = 8.5 Hz, 7H), 3.73 – 3.54 (m, 7H), 3.16 – 3.00 (m, 7H), 2.69 (s, 3H). ^{13}C NMR (100 MHz, $CDCl_3$) δ 161.6, 159.5, 155.4, 154.2, 151.9, 151.6, 150.2, 149.0 (2C), 146.2, 142.9, 141.8, 139.8, 139.6, 136.8, 136.5 (2C), 136.4, 134.2, 134.1, 133.9, 129.8 (2C), 123.0 ((2C), 122.0 (2C), 121.9, 121.8, 117.5, 116.6, 112.2, 111.2, 100.4, 67.9, 59.7 (2C), 55.7, 51.2, 47.5, 46.3, 37.4, 34.9, 34.5, 24.7.

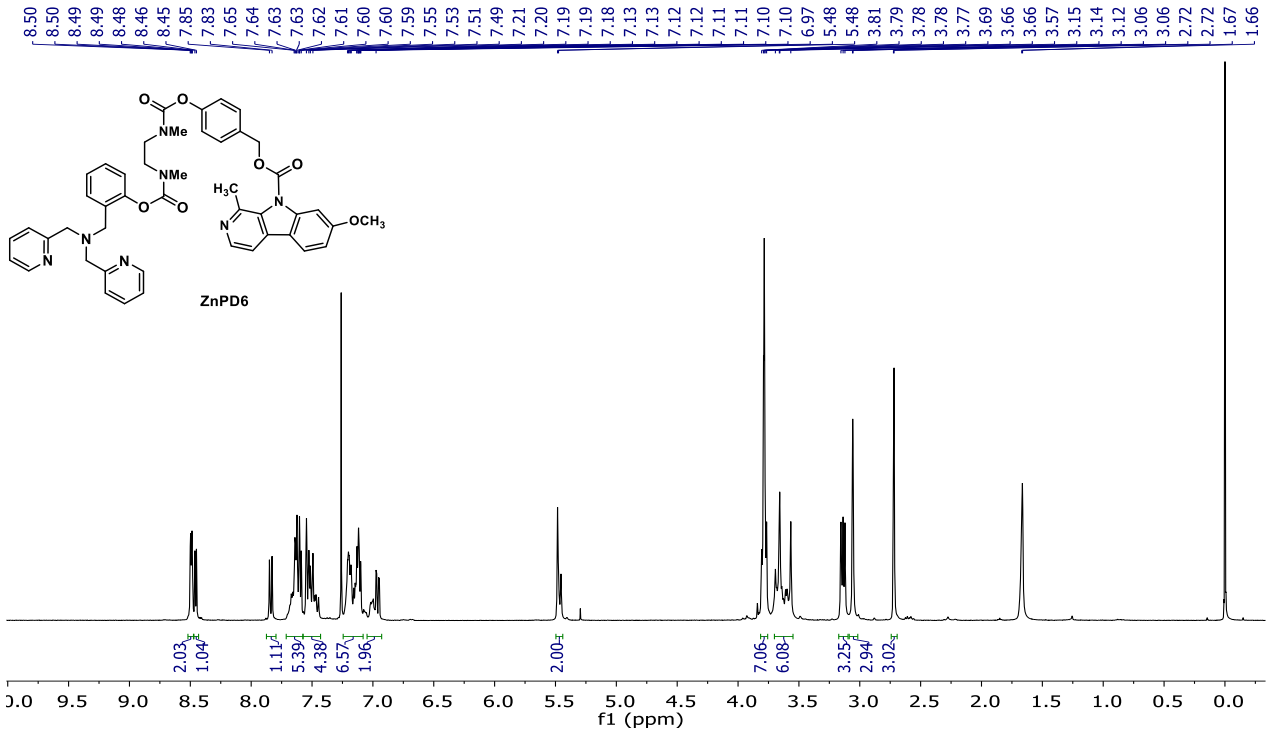

^{1}H NMR spectrum of ZnPD6

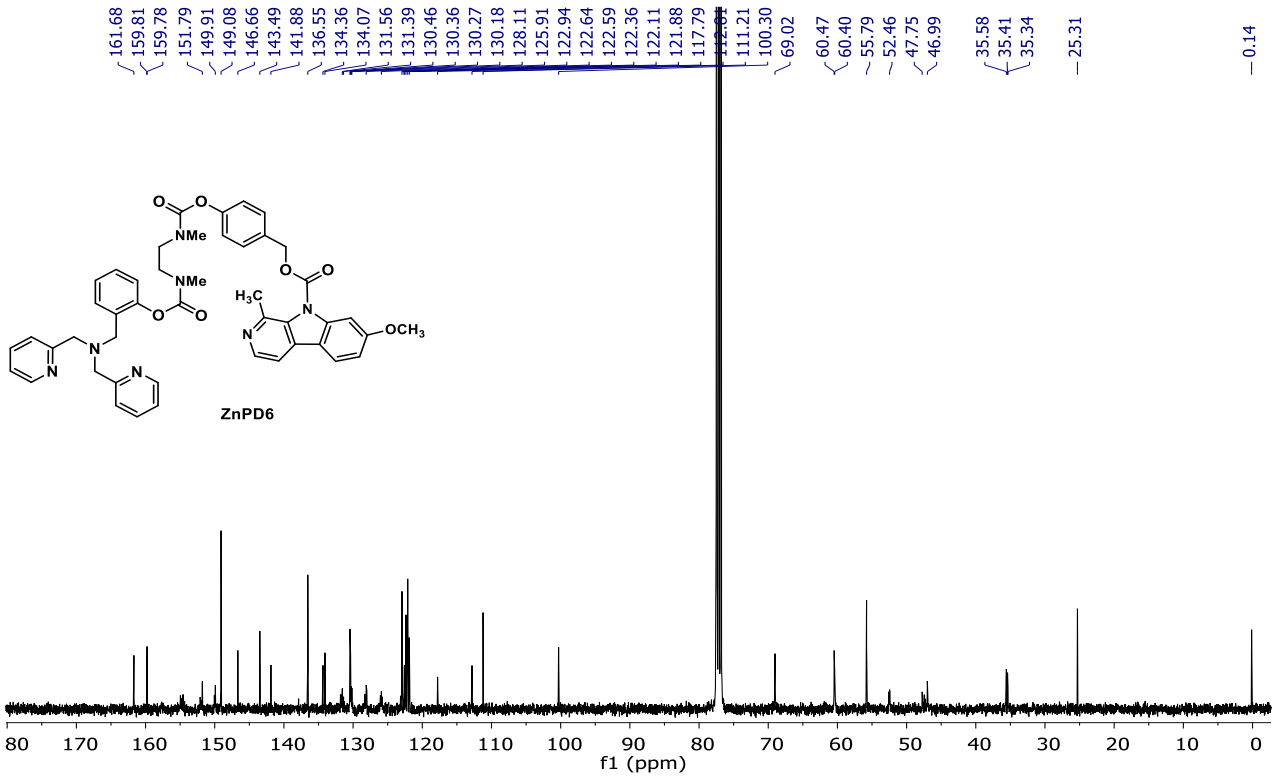

^{13}C NMR spectrum of ZnPD6

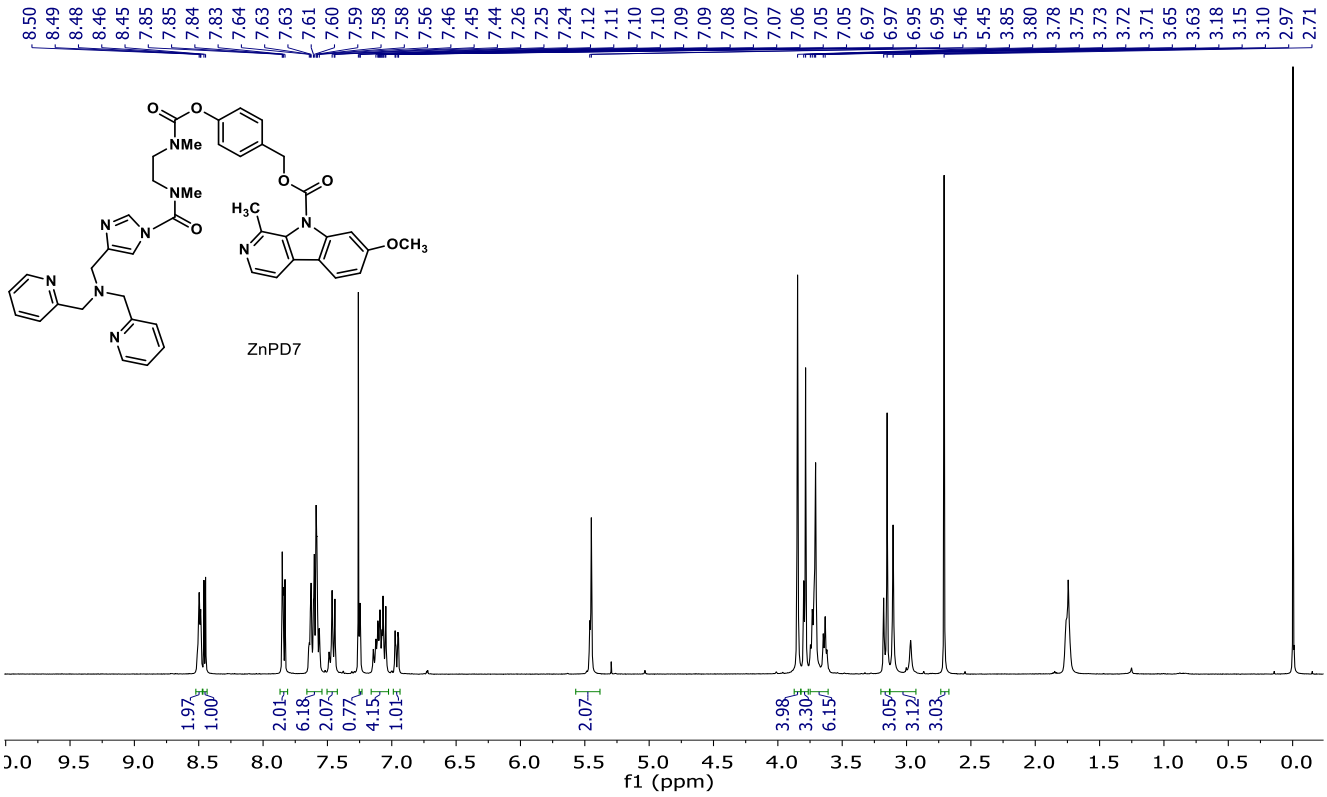

^{1}H NMR spectrum of ZnPD7

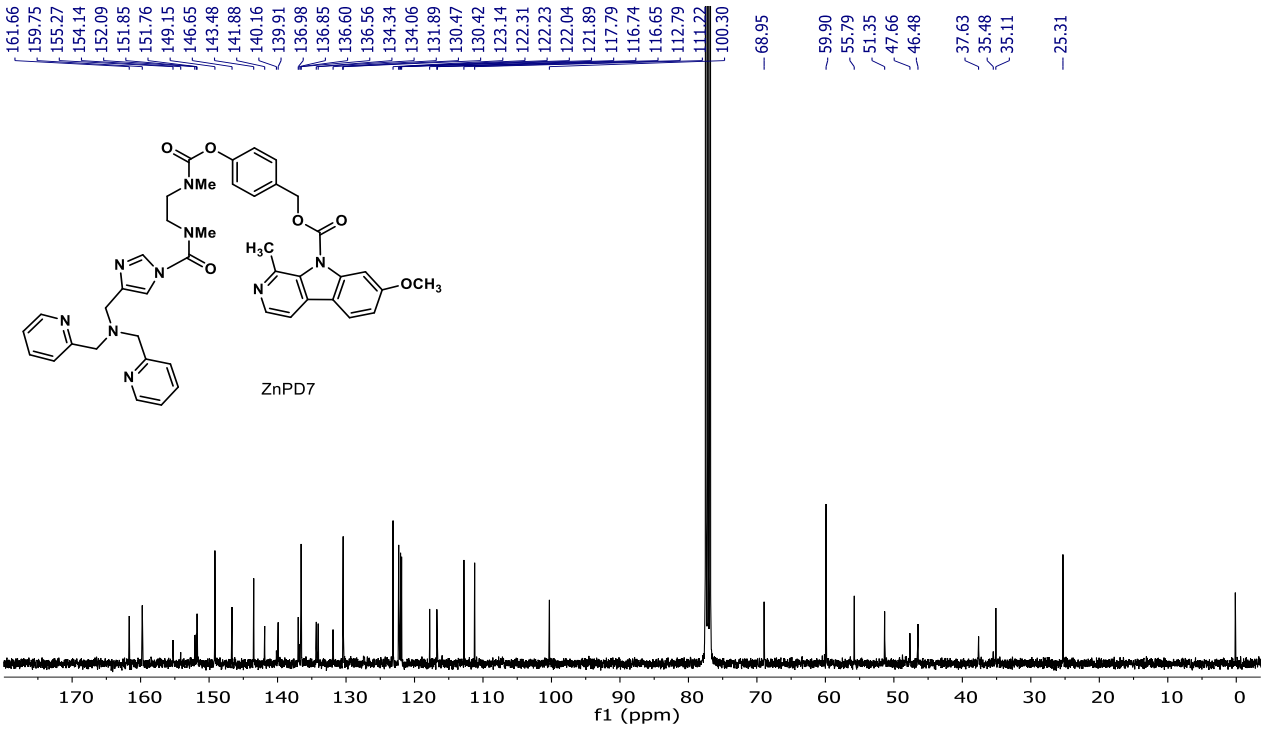

^{13}C NMR spectrum of ZnPD7

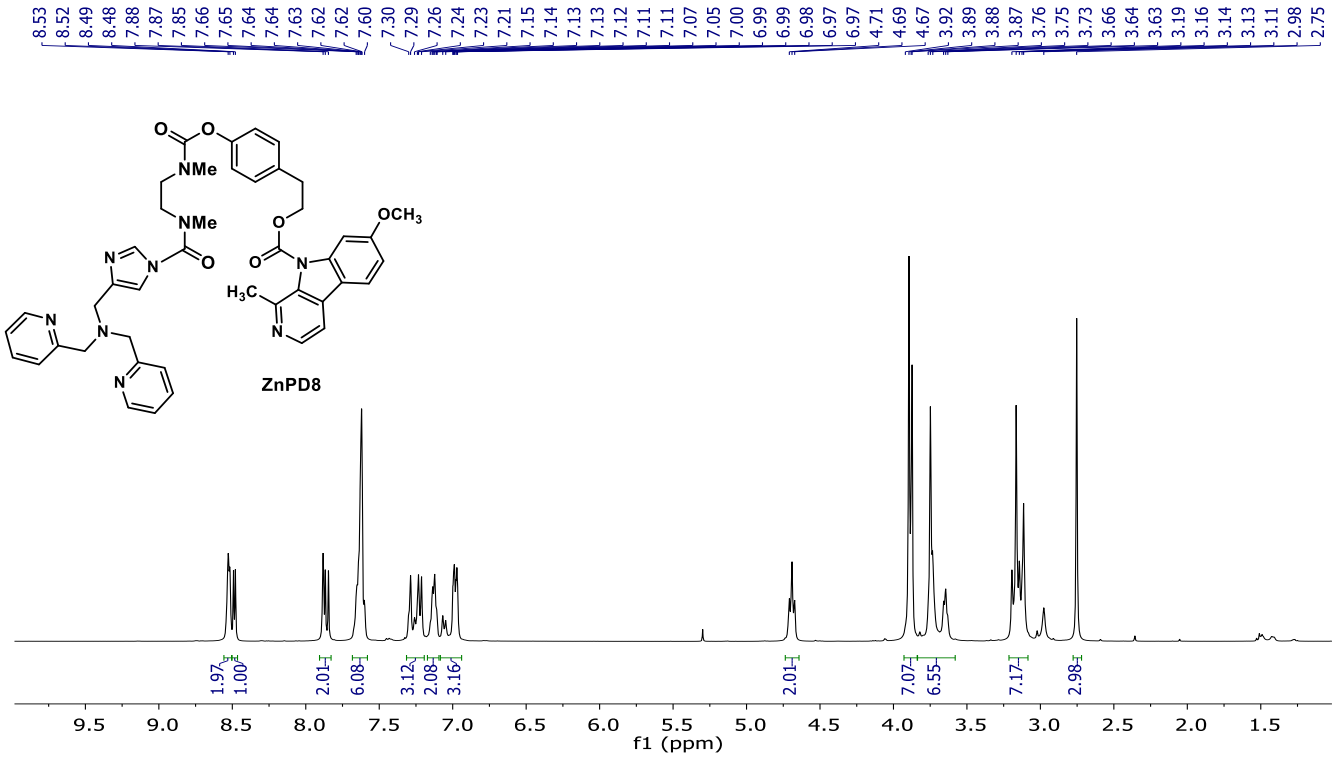

^{1}H NMR spectrum of ZnPD8

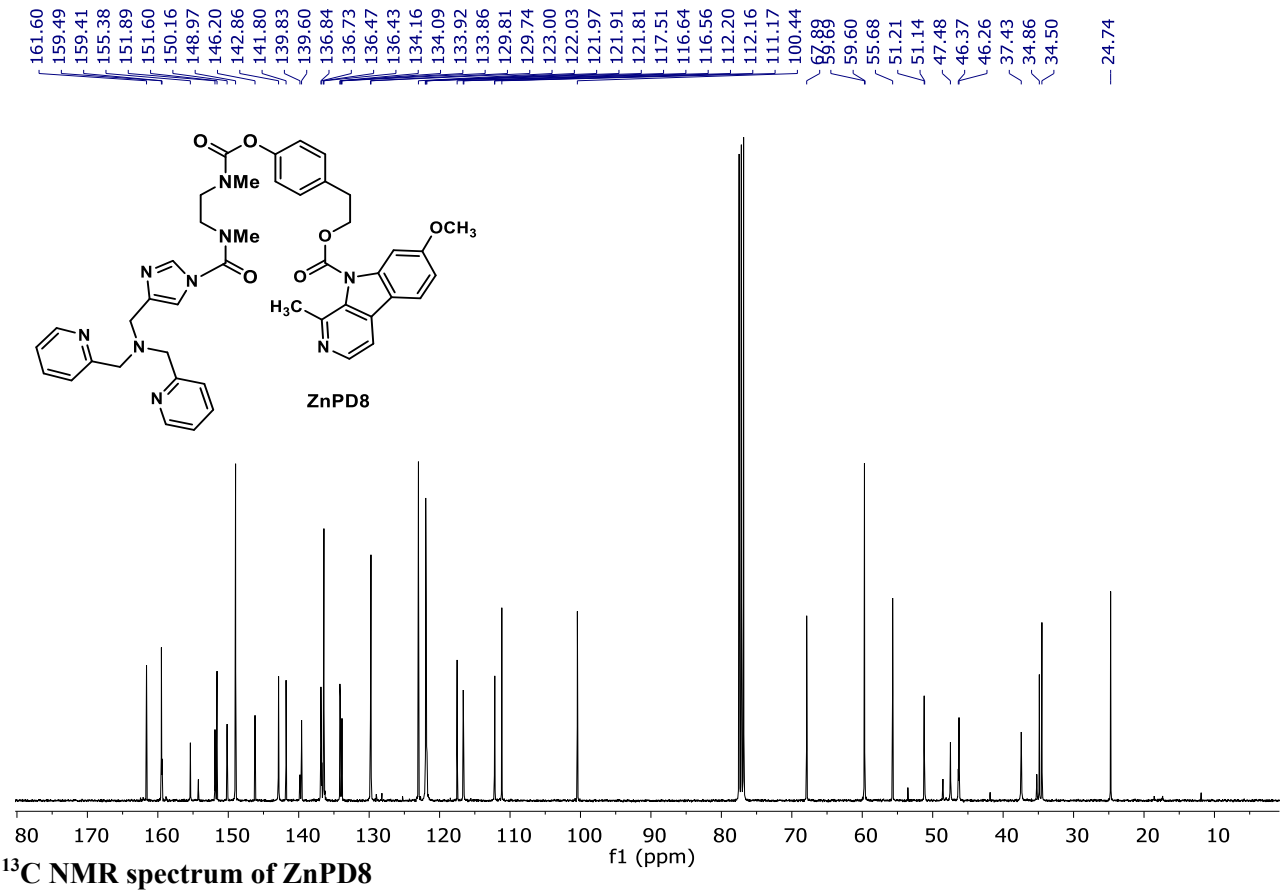

^{13}C NMR spectrum of ZnPD8

REFERENCES AND NOTES

1. A. V. Matveyenko, P. C. Butler, Relationship between β-cell mass and diabetes onset. *Diabetes Obes. Metab.* **10**, 23–31 (2008).

2. J. J. Meier, T. G. K. Breuer, R. C. Bonadonna, A. Tannapfel, W. Uhl, W. E. Schmidt, H. Schrader, Pancreatic diabetes manifests when beta cell area declines by approximately 65% in humans. *Diabetologia* **55**, 1346–1354 (2012).

3. E. A. Ryan, B. W. Paty, P. A. Senior, D. Bigam, E. Alfadhli, N. M. Kneteman, J. R. Lakey, A. M. J. Shapiro, Five-year follow-up after clinical islet transplantation. *Diabetes* **54**, 2060–2069 (2005).

4. N. Lumelsky, O. Blondel, P. Laeng, I. Velasco, R. Ravin, R. McKay, Differentiation of embryonic stem cells to insulin-secreting structures similar to pancreatic islets. *Science* **292**, 1389–1394 (2001).

5. B. Soria, E. Roche, G. Berná, T. León-Quinto, J. A. Reig, F. Martin, Insulin-secreting cells derived from embryonic stem cells normalize glycemia in streptozotocin-induced diabetic mice. *Diabetes* **49**, 157–162 (2000).

6. D. Zhang, W. Jiang, M. Liu, X. Sui, X. Yin, S. Chen, Y. Shi, H. Deng, Highly efficient differentiation of human ES cells and iPS cells into mature pancreatic insulin-producing cells. *Cell Res.* **19**, 429–438 (2009).

7. H. Zulewski, E. J. Abraham, M. J. Gerlach, P. B. Daniel, W. Moritz, B. Müller, M. Vallejo, M. K. Thomas, J. F. Habener, Multipotential nestin-positive stem cells isolated from adult pancreatic islets differentiate ex vivo into pancreatic endocrine, exocrine, and hepatic phenotypes. *Diabetes* **50**, 521–533 (2001).

8. J. Jiménez, L. Riverón-Negrete, F. Abdullaev, J. Espinosa-Aguirre, R. Rodríguez-Arnaiz, Cytotoxicity of the β-carboline alkaloids harmine and harmaline in human cell assays in vitro. *Exp. Toxicol. Pathol.* **60**, 381–389 (2008).

9. L. Egefjord, A. B. Petersen, A. M. Bak, J. Rungby, Zinc, alpha cells and glucagon secretion. *Curr. Diabetes Rev.* **6**, 52–57 (2010).

10. A. Solomou, G. Meur, E. Bellomo, D. J. Hodson, A. Tomas, S. Migrenne Li, E. Philippe, P. L. Herrera, C. Magnan, G. A. Rutter, The zinc transporter Slc30a8/ZnT8 is required in a subpopulation of pancreatic α-cells for hypoglycemia-induced glucagon secretion. *J. Biol. Chem.* **290**, 21432–21442 (2015).

11. K. Lemaire, F. Chimienti, F. Schuit, Zinc transporters and their role in the pancreatic β-cell. *J. Diabetes Investig.* **3**, 202–211 (2012).

12. Y. V. Li, Zinc and insulin in pancreatic beta-cells. *Endocrine* **45**, 178–189 (2014).

13. K. Ramachandran, S. J. Williams, H.-H. Huang, L. Novikova, L. Stehno-Bittel, Engineering islets for improved performance by optimized reaggregation in a micromold. *Tissue Eng. Part A* **19**, 604–612 (2012).

14. H.-C. Chang, C.-H. Lin, D. Juang, H.-W. Wu, C.-Y. Lee, C. Chen, C.-H. Hsu, Multilayer architecture microfluidic network array for combinatorial drug testing on 3D-cultured cells. *Biofabrication* **11**, 035024 (2019).

15. K. Yang, S. Han, Y. Shin, E. Ko, J. Kim, K. I. Park, S. Chung, S. W. Cho, A microfluidic array for quantitative analysis of human neural stem cell self-renewal and differentiation in three-dimensional hypoxic microenvironment. *Biomaterials* **34,** 6607–6614 (2013).

16. J. Amin, K. Ramachandran, S. J. Williams, A. Lee, L. Novikova, L. Stehno-Bittel, A simple, reliable method for high-throughput screening for diabetes drugs using 3D β-cell spheroids. *J. Pharmacol. Toxicol. Methods* **82**, 83–89 (2016).

17. P. Wang, J.-C. Alvarez-Perez, D. P. Felsenfeld, H. Liu, S. Sivendran, A. Bender, A. Kumar, R. Sanchez, D. K. Scott, A. Garcia-Ocana, A. F. Stewart, A high-throughput chemical screen reveals that harmine-mediated inhibition of DYRK1A increases human pancreatic beta cell replication. *Nat. Med.* **21**, 383–388 (2015).

18. J. C. Stendahl, D. B. Kaufman, S. I. Stupp, Extracellular matrix in pancreatic islets: Relevance to scaffold design and transplantation. *Cell Transplant.* **18**, 1–12 (2009).

19. K. I. Aamodt, A. C. Powers, Signals in the pancreatic islet microenvironment influence β-cell proliferation. *Diabetes Obes. Metab.* **19** Suppl 1, 124–136 (2017).

20. M. Kragl, E. Lammert, in *The Islets of Langerhans,* M. S. Islam, Ed. (Springer Netherlands, Dordrecht, 2010).

21. M. Lee, K. Yang, Y. H. Hwang, Y. Byun, D. Y. Lee, S.-W. Cho, H. Lee, Spheroform: Therapeutic spheroid-forming nanotextured surfaces inspired by desert beetle *Physosterna cribripes*. *Adv. Healthc. Mater.* **4**, 511–515 (2015).

22. F. W. Pagliuca, J. R. Millman, M. Gürtler, M. Segel, A. Van Dervort, J. H. Ryu, Q. P. Peterson, D. Greiner, D. A. Melton, Generation of functional human pancreatic β cells in vitro. *Cell* **159**, 428–439 (2014).

23. K. Polonsky, B. Frank, W. Pugh, A. Addis, T. Karrison, P. Meier, H. Tager, A. Rubenstein, The limitations to and valid use of C-peptide as a marker of the secretion of insulin. *Diabetes* **35**, 379–386 (1986).

24. P. J. Carolan, D. A. Melton, New findings in pancreatic and intestinal endocrine development to advance regenerative medicine. *Curr. Opin. Endocrinol. Diabetes Obes.* **20**, 1–7 (2013).

25. X.-Y. Li, W.-J. Zhai, C.-B. Teng, Notch signaling in pancreatic development. *Int. J. Mol. Sci.* **17**, 48 (2016).

26. L. C. Murtaugh, B. Z. Stanger, K. M. Kwan, D. A. Melton, Notch signaling controls multiple steps of pancreatic differentiation. *Proc. Natl. Acad. Sci. U.S.A.* **100**, 14920–14925 (2003).

27. P. A. Seymour, K. K. Freude, M. N. Tran, E. E. Mayes, J. Jensen, R. Kist, G. Scherer, M. Sander, SOX9 is required for maintenance of the pancreatic progenitor cell pool. *Proc. Natl. Acad. Sci. U.S.A.* **104**, 1865–1870 (2007).

28. H. Song, Y. Zhang, Regulation of pancreatic stellate cell activation by Notch3. *BMC Cancer* **18**, 36 (2018).

29. X.-F. Zhang, R.-q. Sun, Y.-f. Jia, Q. Chen, R.-F. Tu, K.-k. Li, X.-D. Zhang, R.-L. Du, R.-h. Cao, Synthesis and mechanisms of action of novel harmine derivatives as potential antitumor agents. *Sci. Rep.* **6**, 33204 (2016).

30. X. Yang, W. Wang, J.-J. Qin, M.-H. Wang, H. Sharma, J. K. Buolamwini, H. Wang, R. Zhang, JKA97, a novel benzylidene analog of harmine, exerts anti-cancer effects by inducing G1 arrest, apoptosis, and p53-independent up-regulation of p21. *PLOS ONE* **7**, e34303 (2012).

31. K. Kumar, P. Wang, R. Sanchez, E. A. Swartz, A. F. Stewart, R. J. DeVita, Development of kinase-selective, harmine-based DYRK1A inhibitors that induce pancreatic human β-cell proliferation. *J. Med. Chem.* **61**, 7687–7699 (2018).

32. J. Shirakawa, R. N. Kulkarni, Novel factors modulating human β-cell proliferation. *Diabetes Obes. Metab.* **18** Suppl 1, 71–77 (2016).

33. Y. J. Wang, M. L. Golson, J. Schug, D. Traum, C. Liu, K. Vivek, C. Dorrell, A. Naji, A. C. Powers, K.-M. Chang, M. Grompe, K. H. Kaestner, Single-cell mass cytometry analysis of the human endocrine pancreas. *Cell Metab.* **24**, 616–626 (2016).

34. M. Lee, B. Maji, D. Manna, S. Kahraman, R. M. Elgamal, J. Small, P. Kokkonda, A. Vetere, J. M. Goldberg, S. J. Lippard, R. N. Kulkarni, B. K. Wagner, A. Choudhary, Native zinc catalyzes selective and traceless release of small molecules in β-cells. *J. Am. Chem. Soc.* **142**, 6477–6482 (2020).

35. W. Chyan, D. Y. Zhang, S. J. Lippard, R. J. Radford, Reaction-based fluorescent sensor for investigating mobile Zn^{2+} in mitochondria of healthy versus cancerous prostate cells. *Proc. Natl. Acad. Sci. U.S.A.* **111**, 143–148 (2014).

36. A. Veres, A. L. Faust, H. L. Bushnell, E. N. Engquist, J. H.-R. Kenty, G. Harb, Y.-C. Poh, E. Sintov, M. Gürtler, F. W. Pagliuca, Q. P. Peterson, D. A. Melton, Charting cellular identity during human in vitro β-cell differentiation. *Nature* **569**, 368–373 (2019).

37. G. Kim, K.-H. Shin, E.-K. Pae, Zinc up-regulates insulin secretion from β cell-like cells derived from stem cells from human exfoliated deciduous Tooth (SHED). *Int. J. Mol. Sci.* **17**, 2092 (2016).

38. K. G. Slepchenko, N. A. Daniels, A. Guo, Y. V. Li, Autocrine effect of Zn^{2+} on the glucose-stimulated insulin secretion. *Endocrine* **50**, 110–122 (2015).

39. K. Rüben, A. Wurzlbauer, A. Walte, W. Sippl, F. Bracher, W. Becker, Selectivity profiling and biological activity of novel β-carbolines as potent and selective DYRK1 kinase inhibitors. *PLOS ONE* **10**, e0132453 (2015).

40. O. Maguire, K. M. Tornatore, K. L. O'Loughlin, R. C. Venuto, H. Minderman, Nuclear translocation of nuclear factor of activated T cells (NFAT) as a quantitative pharmacodynamic parameter for tacrolimus. *Cytometry A* **83**, 1096–1104 (2013).

41. J. Friedrich, C. Seidel, R. Ebner, L. A. Kunz-Schughart, Spheroid-based drug screen: Considerations and practical approach. *Nat. Protoc.* **4**, 309– 324 (2009).

42. P. R. Baraniak, T. C. McDevitt, Scaffold-free culture of mesenchymal stem cell spheroids in suspension preserves multilineage potential. *Cell Tissue Res.* **347**, 701–711 (2012).

43. S.-H. Lee, E. Hao, A. Y. Savinov, I. Geron, A. Y. Strongin, P. Itkin-Ansari, Human β-cell precursors mature into functional insulin-producing cells in an immunoisolation device: Implications for diabetes cell therapies. *Transplantation* **87**, 983–991 (2009).

44. A. Chowdhury, V. P. Satagopam, L. Manukyan, K. A. Artemenko, Y. M. E. Fung, R. Schneider, J. Bergquist, P. Bergsten, Signaling in insulin-secreting MIN6 pseudoislets and monolayer cells. *J. Proteome Res.* **12**, 5954–5962 (2013).

45. K. Yang, S. J. Yu, J. S. Lee, H.-R. Lee, G.-E. Chang, J. Seo, T. Lee, E. Cheong, S. G. Im, S.-W. Cho, Electroconductive nanoscale topography for enhanced neuronal differentiation and electrophysiological maturation of human neural stem cells. *Nanoscale* **9**, 18737–18752 (2017).

46. R. K. P. Benninger, W. S. Head, M. Zhang, L. S. Satin, D. W. Piston, Gap junctions and other mechanisms of cell-cell communication regulate basal insulin secretion in the pancreatic islet. *J. Physiol.* **589**, 5453–5466 (2011).

47. A. Calabrese, D. Caton, P. Meda, Differentiating the effects of Cx36 and E-cadherin for proper insulin secretion of MIN6 cells. *Exp. Cell Res.* **294**, 379–391 (2004).

48. M. A. Ravier, M. Güldenagel, A. Charollais, A. Gjinovci, D. Caille, G. Söhl, C. B. Wollheim, K. Willecke, J.-C. Henquin, P. Meda, Loss of connexin36 channels alters β-cell coupling, islet synchronization of glucose-induced Ca^{2+} and insulin oscillations, and basal insulin release. *Diabetes* **54**, 1798–1807 (2005).

49. J. Kim, I. K. Shim, D. G. Hwang, Y. N. Lee, M. Kim, H. Kim, S.-W. Kim, S. Lee, S. C. Kim, D.-W. Cho, J. Jang, 3D cell printing of islet-laden pancreatic tissue-derived extracellular matrix bioink constructs for enhancing pancreatic functions. *J. Mater. Chem. B* **7**, 1773–1781 (2019).

50. A. Chowdhury, O. Dyachok, A. Tengholm, S. Sandler, P. Bergsten, Functional differences between aggregated and dispersed insulin-producing cells. *Diabetologia* **56**, 1557–1568 (2013).

51. Z. Li, H. Sun, J. Zhang, H. Zhang, F. Meng, Z. Cui, Development of in vitro 3D TissueFlex® islet model for diabetic drug efficacy testing. *PLOS ONE* **8**, e72612 (2013).

52. F. Chimienti, S. Devergnas, F. Pattou, F. Schuit, R. Garcia-Cuenca, B. Vandewalle, J. Kerr-Conte, L. Van Lommel, D. Grunwald, A. Favier, M. Seve, In vivo expression and functional characterization of the zinc transporter ZnT8 in glucose-induced insulin secretion. *J. Cell Sci.* **119**, 4199–4206 (2006).

53. Y. Ichihara, R. Utoh, M. Yamada, T. Shimizu, Y. Uchigata, Size effect of engineered islets prepared using microfabricated wells on islet cell function and arrangement. *Heliyon* **2**, e00129 (2016).

54. O. G. Kelly, M. Y. Chan, L. A. Martinson, K. Kadoya, T. M. Ostertag, K. G. Ross, M. Richardson, M. K. Carpenter, K. A. D'Amour, E. Kroon, M. Moorman, E. E. Baetge, A. G. Bang, Cell-surface markers for the isolation of pancreatic cell types derived from human embryonic stem cells. *Nat. Biotechnol.* **29**, 750–756 (2011).

55. J. B. Gurdon, A. Mitchell, D. Mahony, Direct and continuous assessment by cells of their position in a morphogen gradient. *Nature* **376**, 520–521 (1995).

56. J. B. Gurdon, P. Harger, A. Mitchell, P. Lemaire, Activin signalling and response to a morphogen gradient. *Nature* **371**, 487–492 (1994).

57. C. A. Fraker, S. Alvarez, P. Papadopoulos, J. Giraldo, W. Gu, C. Ricordi, L. Inverardi, J. Domínguez-Bendala, Enhanced oxygenation promotes β-cell differentiation in vitro. *Stem Cells* **25**, 3155–3164 (2007).

58. A. Lindström, J. Carlsson, Penetration and binding of epidermal growth factor-dextran conjugates in spheroids of human glioma origin. *Cancer Biother.* **8**, 145–158 (1993).

59. M. A. Dewit, E. R. Gillies, A cascade biodegradable polymer based on alternating cyclization and elimination reactions. *J. Am. Chem. Soc.* **131**, 18327–18334 (2009).

60. D. Song, J. M. Lim, S. Cho, S. J. Park, J. Cho, D. Kang, S. G. Rhee, Y. You, W. Nam, A fluorescence turn-on H_2O_2 probe exhibits lysosome-localized fluorescence signals. *Chem. Commun. (Camb.)* **48**, 5449–5451 (2012).

61. Y. Lee, G. Y. Park, H. R. Lucas, P. L. Vajda, K. Kamaraj, M. A. Vance, A. E. Milligan, J. S. Woertink, M. A. Siegler, A. A. Narducci Sarjeant, L. N. Zakharov, A. L. Rheingold, E. I. Solomon, K. D. Karlin, Copper(I)/O_2 chemistry with imidazole containing tripodal tetradentate ligands leading to μ-1,2-peroxo-dicopper(II) species. *Inorg. Chem.* **48**, 11297–11309 (2009).